https://doi.org/10.5194/egusphere-2026-5718
Preprint. Discussion started: 15 October 2026
© Author(s) 2026. CC BY 4.0 License.

# Importance of emissions-driven simulation of methane for representation of key atmospheric oxidants

Xuewei Hou[1,2*], Ryan Hossaini[1*], Oliver Wild[1], James Lee[3,4], Ye Wang[1]

[1]Lancaster Environment Centre, Lancaster University, Lancaster, LA1 4YW, UK.

[2]Collaborative Innovation Center on Forecast and Evaluation of Meteorological Disasters, School of Atmospheric Physics, Nanjing University of Information Science and Technology, Nanjing, 210044, China.

[3]Department of Chemistry, University of York, York, YO10 5DD, UK.

[4]National Centre for Atmospheric Science, University of York, York, YO10 5DD, UK.

***Correspondence:** Xuewei Hou (houxw@nuist.edu.cn) and Ryan Hossaini (r.hossaini@lancaster.ac.uk)

**Abstract**: Methane ($CH_4$) is a major greenhouse gas influencing both climate and atmospheric chemistry through its interactions with hydroxyl radicals (OH) and ozone ($O_3$). Using the FRSGC/UCI chemical transport model, we compare a new emission-driven simulation with configurations where $CH_4$ mixing ratios are prescribed at the surface or throughout the troposphere. The emission-driven simulation better reproduces the observed spatiotemporal characteristics of $CH_4$ and captures stronger positive trends over major source regions. With a global $CH_4$ source of 602 $Tg \cdot yr^{-1}$ we find sinks of 515 $Tg \cdot yr^{-1}$ from tropospheric chemical loss and ~36 $Tg \cdot yr^{-1}$ each from soil uptake and stratospheric loss. The impact of $CH_4$ treatment on global oxidants is modest, with tropospheric $O_3$ and OH burdens 0.6% and 0.05% higher in the emission-driven simulation, respectively. The simulated $CH_4$–OH feedback is insensitive to the choice of $CH_4$ configuration, with conventional feedback factors ranging from 1.403 to 1.409 across the three configurations. However, there is a pronounced influence on the longer-term response to emission perturbations. A 20% reduction in surface NO emissions produces immediate decreases in $O_3$ and OH, but the emission-driven simulation additionally captures the persistent response in $CH_4$ burden, which peaks at 21.5 Tg in the following year and decays with a perturbation lifetime of 12.5 years. The elevated $CH_4$ enhances $O_3$, partially offsetting its initial decrease. These results demonstrate that an emission-driven treatment provides a more complete framework for quantifying long-term $CH_4$–OH–$O_3$ responses to emission changes and assessing their impacts on atmospheric chemistry and climate.

**Keywords**: Methane; Atmospheric chemistry model; Emissions; Boundary condition; Feedback

## 1 Introduction

Methane ($CH_4$) is the second most important anthropogenic greenhouse gas after carbon dioxide, with a global warming potential approximately 28–34 times greater on a 100-year time horizon (Myhre et al., 2013). Its atmospheric concentration has more than doubled since pre-industrial times, making it a major driver of climate change (Dlugokencky et al., 2011; Lan et al., 2025). Beyond its direct radiative forcing, $CH_4$ also influences atmospheric chemistry by affecting tropospheric ozone ($O_3$) and stratospheric water vapor, contributing additional indirect climate effects (Holmes et al., 2013; Turner et al., 2016; Stevenson et al., 2020). $CH_4$ has both natural and anthropogenic sources. Natural emissions are dominated by wetlands, which account for 24–29% of the global total source of global

https://doi.org/10.5194/egusphere-2026-5718
Preprint. Discussion started: 15 October 2026
© Author(s) 2026. CC BY 4.0 License.

emissions (Zhang et al., 2023; Saunois et al., 2025). Recent satellite-based and inversion analyses have highlighted that tropical wetlands—particularly in the Congo Basin, Amazon, and Southeast Asia—are releasing substantially more $CH_4$ than previously estimated, playing a key role in the renewed growth of atmospheric $CH_4$ since 2007 (Bloom et al., 2017; Wilson et al., 2021; Murguia-Flores et al., 2023; Lin et al., 2024). Anthropogenic contributions stem primarily from agriculture, fossil fuel production, and waste management (Jackson et al., 2020; Nisbet et al., 2023; Saunois et al., 2025). The spatial and temporal variability of these emissions, combined with large uncertainties in sinks such as soil uptake and oxidation by hydroxyl radicals (OH), complicates accurate $CH_4$ budget assessments (Holmes et al., 2013; Nisbet et al., 2019).

Regional $CH_4$ emissions are uncertain due to sparse observational constraints. Ground-based monitoring networks remain limited in some regions, especially the tropics, while satellite products, though improving, still face retrieval and coverage limitations (Jacob et al., 2022; Qu et al., 2021). Despite these challenges, progress in satellite remote sensing and atmospheric inversions has enhanced our ability to quantify emissions and identify regional hotspots (Bloom et al., 2017). However, discrepancies between top-down and bottom-up approaches remain a central uncertainty in quantifying the $CH_4$ budget (Saunois et al., 2020, 2025; Jackson et al., 2020).

In chemical transport model (CTM) and earth system model (ESM) studies, $CH_4$ is most commonly included by prescribing surface mixing ratios. This ensures that concentrations match observations and do not drift under the effects of uncertainty in emissions or biases in chemical removal associated with imperfect representation of OH. Ten of the fourteen global models that contributed to the Atmospheric Chemistry and Climate Model Intercomparison Project (ACCMIP) and all models that performed hindcast runs for Phase 6 of the Coupled Model Intercomparison Project (CMIP6) adopted this approach (Voulgarakis et al., 2013; Griffiths et al., 2021). Beyond $CH_4$, the approach is widely adopted for a range of other long-lived gases and the observational constraint it provides is a major advantage. However, $CH_4$ boundary conditions are typically provided in discrete latitude bins, and thus zonal variability and emission hot spots are not represented.

Emission-driven simulations offer a more process-based representation of $CH_4$ sources and enable the geographical attribution of atmospheric $CH_4$ and its trends to different source regions and emission sectors (Szopa et al., 2013; Stanevich et al., 2020; Folberth et al., 2022). While emission-driven simulations have been shown to be viable (e.g. Patra et al., 2011), a major challenge with this approach is that simulated $CH_4$ concentrations drift from reality due to biases in the emissions and weaknesses in model representation of tropospheric OH, the primary $CH_4$ sink. To address this some studies have implemented online 'flux adjustment' schemes by altering the magnitude of $CH_4$ emissions to ensure that mixing ratios remain close to those observed (e.g., Folberth et al. 2022).

Another challenge in driving atmospheric models with $CH_4$ emissions is the feedback of $CH_4$ on OH and $O_3$. $CH_4$ oxidation consumes OH, which alters the oxidative capacity of the troposphere (Stevenson et al., 2020; Zhao et al., 2020; Zhao et al., 2025). As OH is the primary sink for $CH_4$, this process constitutes a chemical feedback that influences $CH_4$ atmospheric lifetime and contributes to nonlinearities in its projected concentrations (Stecher et al., 2021). Additionally, $CH_4$ oxidation leads to formation of formaldehyde and carbon monoxide (CO), which can enhance tropospheric $O_3$ formation, particularly under polluted conditions (Voulgarakis et al., 2013; Turner et al., 2016). Holmes (2018) compared $CH_4$ lifetime and feedback under three approaches to representing $CH_4$ and found that differences in feedback factors were very small, although an emission-driven configuration exhibits the strongest feedback. Emissions of hydrocarbons and CO were shown to weaken the $CH_4$ feedback, whereas nitrogen oxide ($NO_x$) emissions have a more complex effect, reducing $CH_4$

https://doi.org/10.5194/egusphere-2026-5718
Preprint. Discussion started: 15 October 2026
© Author(s) 2026. CC BY 4.0 License.

feedback over source regions but enhancing it elsewhere. In contrast, Voulgarakis et al. (2013) reported that declining anthropogenic $NO_x$ emissions contribute to a projected strengthening of the $CH_4$ feedback through the twenty-first century under the RCP8.5 scenario.

Global atmospheric chemistry model simulations consistently show that decreases in $NO_x$ emissions reduce OH concentrations and prolong the global methane lifetime (Derwent et al., 2001; Wild et al., 2001; Stevenson et al., 2004; Weber et al., 2020). Although $CH_4$ has an atmospheric lifetime of roughly 10 years, model studies demonstrate that it responds rapidly to sudden, short-lived $NO_x$ emission pulses within a few months (Wild et al., 2001; Stevenson et al., 2004). Stevenson et al. (2022) further demonstrated that the abrupt emission changes during the COVID-19 lockdowns rapidly affected the global $CH_4$ growth rate, with $NO_x$ emission reductions contributing to an increase of $4.8 \pm 1.0$ ppb·yr$^{-1}$. While the overall methane feedback is reasonably well constrained, the coupled $CH_4$–$O_3$–OH response to emission perturbations remains uncertain and requires further quantitative investigation.

Given the uncertainties and limitations associated with $CH_4$ sources, sinks, and its atmospheric behaviour, it is essential to understand how different approaches to representing $CH_4$ in models influences its simulated impacts. This study aims to quantify the effects of three commonly used frameworks—fixed field, fixed surface and emissions-driven approaches—on the spatial and temporal distribution, atmospheric lifetime, and chemical feedback of $CH_4$, particularly in relation to key oxidants such as OH and $O_3$ and its response to $NO_x$ emissions. Using an updated chemical transport model, we conduct a series of simulations to compare these approaches. Section 2 describes the model setup, simulation design, and observational datasets used for evaluation. Model evaluation, differences in $CH_4$ budget and trend, impact on tropospheric oxidants, $CH_4$ chemical feedback, and response to surface $NO_x$ emissions are presented in Section 3, followed by conclusions in Section 4.

## 2 Model and methods

In this section, we provide a brief overview of the CTM in its standard configuration with prescribed 3-D fields of $CH_4$ and the modifications introduced in this study to implement additional configurations based on fixed surface concentrations and on $CH_4$ emissions.

### 2.1 Chemical Transport Model

The global atmospheric model used here is the Frontier Research System for Global Change version of the University of California, Irvine (FRSGC/UCI) CTM. The model is described in Wild and Prather (2000) and has been widely used to study the tropospheric chemistry and transport of trace gases including $O_3$ and OH (e.g. Wild et al., 2020). Results from the model have been included in a range of model intercomparison initiatives, such as the Hemispheric Transport of Air Pollution (HTAP) projects (Fiore et al, 2009). The model was recently updated and extensively evaluated by Hou et al. (2026). The CTM uses offline meteorological data generated with the European Centre for Medium-Range Weather Forecasts (ECMWF) Integrated Forecast System (IFS) version Cy38r1.

### 2.2 Chemistry and Emissions in the Default Configuration

The default configuration of the model used here is the same as that described and evaluated by Hou et al. (2026). Briefly, it includes explicit treatment of $HO_x/O_x/NO_x$ chemistry, $CH_4$ and isoprene oxidation, and a lumped approach for other non-methane hydrocarbons (NMHCs) based on representative species butane, propene and xylene (Wild, 2007). Alongside gas-phase chemistry, the model now includes a detailed treatment of heterogenous chemistry occurring on tropospheric aerosols, cloud liquid water and cloud ice (Hou et al., 2026).

https://doi.org/10.5194/egusphere-2026-5718
Preprint. Discussion started: 15 October 2026
© Author(s) 2026. CC BY 4.0 License.

Monthly emissions of CO, $NO_x$ and NMHCs are prescribed largely from inventories produced by the Copernicus Atmosphere Monitoring Service (CAMS). Anthropogenic emissions are from version 6.2 of the CAMS-GLOB-ANT inventory (Soulie et al., 2024), aircraft emissions from version 2.1 of CAMS-GLOB-AIR (Granier et al., 2019), biogenic emissions from version 3.1 of CAMS-GLOB-BIO (Sindelarova et al., 2022) and soil emissions from version 2.4 of CAMS-GLOB-SOI (Simpson and Darras, 2021). Fire emissions are taken from the Global Fire Emissions Database, Version 4.1 (GFED4s) inventory (van der Werf et al., 2017). Each of the emissions above vary annually over our full simulation period. Oceanic emissions of CO and selected NMHCs are taken from the POET emission inventory and are assumed to be climatological (Granier et al., 2005). Lightning NOx emissions are included in the model and vary annually, providing a source of about 5 $Tg[N]\cdot yr^{-1}$.

### 2.3 Modifications to Represent $CH_4$ Sources and Sinks

In the standard model simulations, an annual and latitudinally varying mixing ratio of $CH_4$ is prescribed using the historical forcing data prepared for CMIP6 until 2014 (Meinshausen et al., 2017). Post 2014, to match the observed record, the fields are scaled by a globally uniform factor derived from $CH_4$ measurements of the National Oceanic and Atmospheric Administration (NOAA) global monitoring network. In this standard configuration of the model (STD_Fix), the $CH_4$ mixing ratios are prescribed uniformly through the depth of the troposphere. For an alternate configuration (STD), we prescribe $CH_4$ mixing ratios at the surface only and allow model transport processes to define concentrations above the surface.

For an emission-driven configuration (CH4E), we have replaced the prescribed $CH_4$ mole fractions with explicit monthly emissions. Six $CH_4$ source types are included: anthropogenic, wetland, geological, termite, fire, and biogenic emissions. The annual global emission totals are shown in **Figure 1**, and the spatial distribution is shown in **Figure S1**. For the anthropogenic source, we adopt the $CH_4$ emissions inventory produced for CMIP7 (Hoesly et al., 2025). Wetland emissions are from the high emissions scenario in the extended ensemble subset of Bloom et al. (2017). Fire emissions are from the GFED4s inventory (van der Werf et al., 2017). Biogenic emissions are from CAMS-GLOB-BIO (v3.1) inventory (Sindelarova et al., 2022). Emissions from termites are taken from the CAMS-GLOB-TERM (v1.1) inventory and do not vary annually but are assumed representative of the period 2000 – 2017 (Granier et al., 2019). Estimated geological emissions for the year 2022 are taken from Martinezet al. (2024) and Saunois et al., (2025), and are fixed in time due to limited information on annual variability.

The dominant chemical sink of $CH_4$ in the atmosphere is reaction with OH, which is responsible for 80-90% of the total chemical $CH_4$ loss (Kirschke et al., 2013; Saunois et al., 2025; Folberth et al., 2022). The temperature-dependent rate coefficient for this reaction is taken as $2.45\times10^{-12}\exp(-1775/T)$ $cm^3\cdot molecules^{-1}\cdot s^{-1}$ (Burkholder et al., 2020). Chlorine radicals provide an additional $CH_4$ sink, ~0.8% of global $CH_4$ oxidation (Wang et al., 2021), but this is relatively small and is not included in the model at present. The chemical removal of $CH_4$ in the stratosphere is parameterized using a first-order loss rate above the tropopause, and the $CH_4$ global lifetime to stratospheric loss is approximately 140 years. This estimate is consistent with previous estimates of 120 years in Prather et al. (2012) and 195 (153−270) years in Brown et al. (2013).

https://doi.org/10.5194/egusphere-2026-5718
Preprint. Discussion started: 15 October 2026
© Author(s) 2026. CC BY 4.0 License.

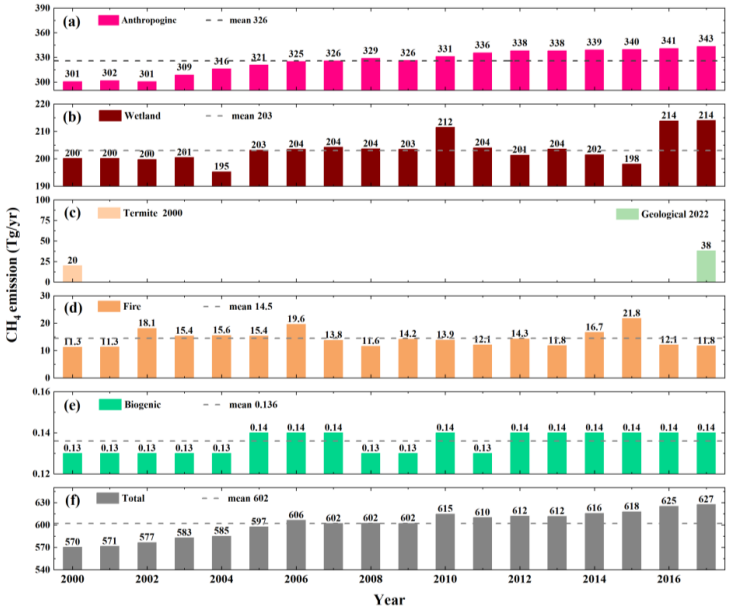


**Figure 1.** Annual $CH_4$ emissions (Tg/yr) implemented in the CH4E configuration of the model (2000-2017). The bottom row (f) shows the global total emissions while rows above show the individual contributions from (a) anthropogenic, (b) wetland, (c) geological and termite, (d) fire, and (e) biogenic sources. In each panel, the dashed horizontal line indicates the mean emission rate over 2000–2017. Geological and termite emissions are time-invariant.

**Table 1.** Typical values of $CH_4$ dry deposition velocities

| Ecosystem type | $V_d$ (*$10^{-6}$ m·$s^{-1}$) |
|---|---|
| Ice and water | 0 |
| Tropical forest | 10.6 |
| Boreal forest | 8.5 |
| Grassland | 7.4 |
| Tundra | 4.8 |
| Desert | 3.5 |
| Cultivation | 3.9 |

For the emissions-driven configuration, we implemented surface soil uptake based on the $CH_4$ dry deposition velocity. Typical values of $CH_4$ dry deposition velocities over different land types are shown in **Table 1** and are calculated from Equation (1) based on the mean uptake rates of $CH_4$ from Dutaur and Verchot (2007).

$$V_{di} = \frac{F_i}{F} \times V_{d0} \times \frac{1}{r} \quad (1)$$

https://doi.org/10.5194/egusphere-2026-5718
Preprint. Discussion started: 15 October 2026
© Author(s) 2026. CC BY 4.0 License.

$V_{di}$ is the $CH_4$ dry deposition velocity to land type $i$; $F_i$ is the mean uptake rate over land type $i$ in Dutaur and Verchot (2007); $F$ is the total mean uptake in Dutaur and Verchot (2007); $V_{d0}$ is the global mean dry deposition velocity, taken here as $3.2 \times 10^{-6}$ m·s$^{-1}$. $r$ is the ratio of land area to the global surface area. Following the approximate global land fraction reported in Zhao et al. (2017), $r$ is taken as 0.30 in this study.

### 2.4 Experimental approach

We performed three model experiments, STD_Fix, STD and CH4E, the main features of which are summarized in **Table 2**. All runs were performed at T42 horizontal resolution (2.8°×2.8°) and with 57 vertical levels extending from the surface to 0.1 hPa. The experiments used the same meteorological conditions and the same emissions for species other than $CH_4$. $CH_4$ mixing ratios were prescribed everywhere in STD_Fix, only in the lowest layers at the surface in STD, and $CH_4$ emissions were used in CH4E. All experiments were run for the period 2000 to 2017. Preceding this, a spin-up of 2.5 years was used for STD_fix and STD experiments, and a longer spin-up of 7.5 years was used to balance the impact of $CH_4$ emissions (CH4E) on other species at the start of the simulation.

**Table 2.** Experimental settings

| | **Run STD_Fix** | **Run STD** | **Run CH4E** |
|---|---|---|---|
| $CH_4$ boundary conditions | Prescribed mole fractions everywhere (Fixed field) | Prescribed mole fractions at the surface (Fixed surface) | 6 sources, total ~602 Tg/yr (specified emissions) |
| Year | 2.5-yr Spin-up; 2000-2017 | 2.5-yr Spin-up; 2000-2017 | 7.5-yr Spin-up; 2000-2017 |
| $CH_4$ Deposition | Updated deposition scheme in section 2.3 | | |
| Stratospheric loss | First-order loss with a rate constant of 0.05 yr$^{-1}$ | | |
| Meteorology | ECMWF Integrated Forecasting System (IFS) model versions Cy38r1 | | |
| Emissions | CAMS-GLOB+GFED4S fire | | |
| Resolution | T42L57 | | |

### 2.5 Observation data

To evaluate model performance, we use monthly surface $CH_4$ measurements and vertical $CH_4$ profiles obtained by the National Oceanic and Atmospheric Administration (NOAA) Global Monitoring Laboratory (GML). A total of 67 surface observation sites with continuous $CH_4$ records spanning the study period (2000-2017) were selected. The site information is provided in **Table S1**, and further details are available in Lan et al. (2025).

Vertical $CH_4$ profile data were obtained through NOAA GML's Aircraft Program, which supports a range of measurement and monitoring activities (McKain et al., 2026). These include routine airborne sampling at fixed sites across the USA under the NOAA GML's Global Greenhouse Gas Reference Network (GGGRN), targeted intensive campaigns, and the National Observations of Greenhouse gases Aircraft Profiles (NOGAP) program. The NOGAP program conducts near-continuous atmospheric sampling around the continental USA with the goal of addressing spatial sampling gaps. In total, vertical profile data from 33 observation sites covering the study period were used. Site-specific information is summarized in **Table S2**.

## 3 Results

### 3.1 Model evaluation

**Figure 2a** compares modeled and observed surface $CH_4$ mixing ratios at 67 NOAA sites, averaged

https://doi.org/10.5194/egusphere-2026-5718
Preprint. Discussion started: 15 October 2026
© Author(s) 2026. CC BY 4.0 License.

over the period 2000–2017, as a function of latitude. Both prescribed and emission-driven configurations generally capture the latitudinal gradient of $CH_4$ well, with higher concentrations in the northern hemisphere than the southern hemisphere, especially between 30°N and 60°N, where emissions are more intense (**Figure S2**). Model biases for the prescribed and emission-driven runs are shown in **Figures 2b** and **2c**, respectively. Surface $CH_4$ concentrations in prescribed concentration runs (STD and STD_Fix) are the same and thus the simulations are not shown separately here. The STD prescribed concentration simulation has a mean bias of −5.7 ± 27.9 ppbv (mean ± 1 standard deviation across the 67 sites), with particularly large negative biases at some sites in the northern hemisphere mid-latitudes (30°N–60°N). This underestimation may arise from the assumption of annual and zonal mean concentrations along latitude. The uncertainty may also be associated with extending the prescribed $CH_4$ concentration data to 2015–2017. The emission-driven CH4E simulation has a positive mean bias of 14.2 ± 19.6 ppbv, but a smaller spatial spread in site-level biases, indicating that explicitly resolving $CH_4$ emissions reduces some of the large regional discrepancies found in the prescribed concentration simulation. While this simulation overestimates $CH_4$ in some regions, especially at mid- to high- latitudes, it better reproduces the observed interhemispheric gradient. For example, the observed interhemispheric gradient from the sites in **Figure 2a** is 102.5 ppbv, compared with 94.7 ppbv in the STD run and 100.4 ppbv in the CH4E run.

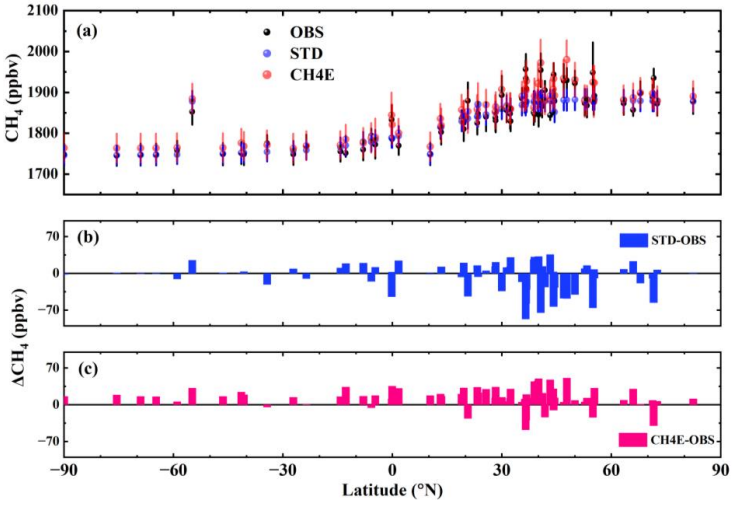


**Figure 2.** (a) Latitudinal distribution of observed and modeled surface $CH_4$ (ppbv) averaged over the period 2000–2017. The observations are from the NOAA GML network (OBS, 67 sites). Model output is shown for STD (fixed surface) and CH4E (emission-driven) runs. (b) and (c) Corresponding model minus observation difference in $CH_4$ (ppbv). Positive values indicate overestimation by the model.

https://doi.org/10.5194/egusphere-2026-5718
Preprint. Discussion started: 15 October 2026
© Author(s) 2026. CC BY 4.0 License.

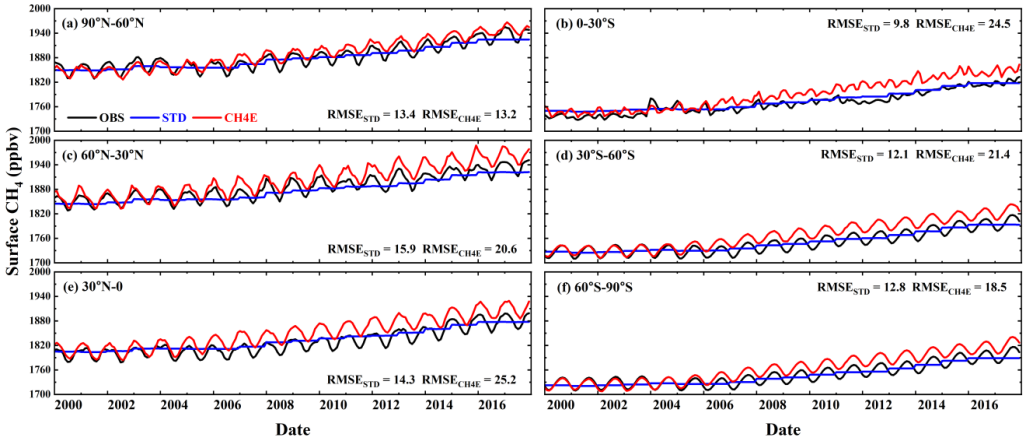


**Figure 3.** Time series of monthly mean surface $CH_4$ (ppbv) from emission-driven (CH4E) and prescribed (STD) simulations against observations in different latitude bands. The root mean square error (RMSE) between the model and observations (ppbv) are labelled in each panel.

240

**Figure 3** shows the time series of modelled surface $CH_4$ mixing ratios from 2000 to 2017, averaged within 30° latitude bands, against observations. The root mean square error (RMSE) for each model run is also shown in each panel. In general, both model runs closely follow the observed $CH_4$ trends during the early years (2000–2004) across all latitude bands. From around 2005 onward, the emission-
245 driven CH4E simulation begins to show a small systematic positive bias relative to the observations, particularly in the tropics and southern hemisphere, suggesting an overestimation of $CH_4$ emissions or underestimation of $CH_4$ sinks in this run. One potential explanation for this discrepancy is the flattening of the OH trend in the model (Hou et al., 2026), which contrasts with the increasing trends observed in other studies. Overall, averaged over our study period the emission-driven simulation
250 yields lower RMSE than the prescribed concentration simulation in the 90°N–60°N band, but higher RMSE in most other latitude bands, particularly in the tropics (30°N–0° and 0°–30°S). However, the magnitude of the biases in the emission-driven simulation are sufficiently small that we do not require an emission flux adjustment of the type described by Folberth et al. (2022).

The emission-driven simulation captures the amplitude and phase of the observed $CH_4$ seasonal cycle
255 extremely well in all latitude bands (**Figure S3**). The prescribed concentration simulation shows no seasonal variation in the anomalies because annual mean surface $CH_4$ mixing ratios are prescribed without a seasonal cycle in this configuration.

https://doi.org/10.5194/egusphere-2026-5718
Preprint. Discussion started: 15 October 2026
© Author(s) 2026. CC BY 4.0 License.

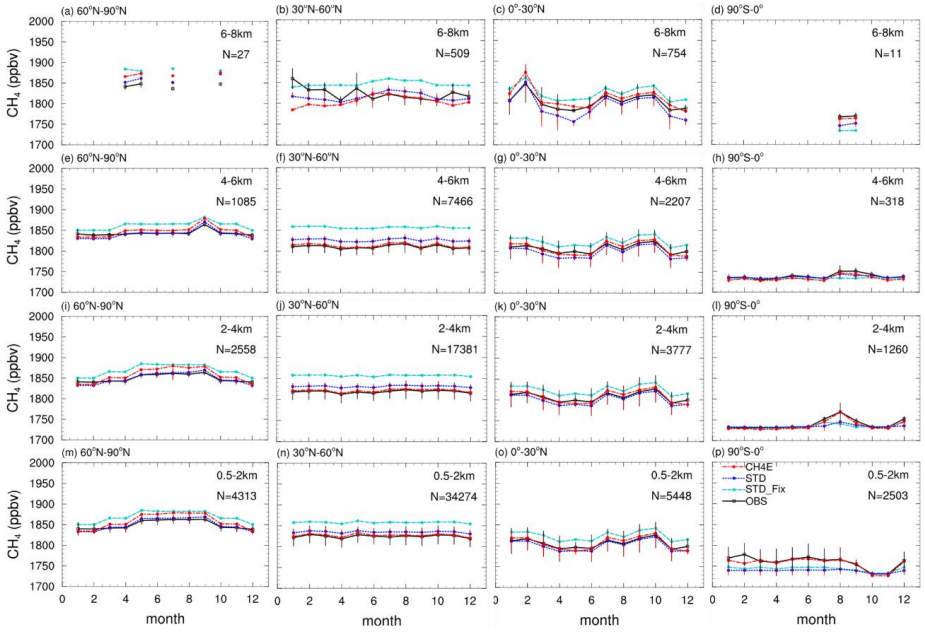


**Figure 4.** Multi-year averaged monthly variations in simulated and observed $CH_4$ mixing ratio (ppbv) from 2000 to 2017 for different latitude bands and four altitude ranges: 0.5–2 km, 2–4 km, 4–6 km, and 6–8 km (bottom to top). Observational data are from NOAA's aircraft measurement program using discrete flask-air samples collected at multiple altitudes. N indicates the number of samples used in each dataset.

To further evaluate the vertical and seasonal variations in $CH_4$, **Figure 4** compares the simulated and observed monthly $CH_4$ mixing ratios over 2000–2017 across four latitude bands and altitude ranges. As $CH_4$ in the fully prescribed simulation is fixed to an annual-mean distribution, the apparent monthly variations in this simulation arise from differences in the spatial and temporal sampling of the observations rather than from simulated seasonal variability. The prescribed-surface and emission-driven simulations generally reproduce the observed variations across the different latitude and altitude ranges, including the large-scale latitudinal gradient, with higher $CH_4$ mixing ratios in the northern hemisphere than in the southern hemisphere, and the latitude-dependent seasonal variations. The two simulations show similar vertical and seasonal patterns, with the emission-driven simulation generally showing closer agreement with the observed $CH_4$ mixing ratios. These results further indicate that explicitly resolving $CH_4$ emissions and sinks can reproduce the observed large-scale vertical, latitudinal, and seasonal characteristics reasonably well.

### 3.2 $CH_4$ global budget

The global $CH_4$ budget averaged over the periods 2000-2009 and 2010-2017 from the three model simulations and from recent literature studies over similar periods (Saunois et al., 2025; Folberth et al., 2022) are compared in **Table 3**. All budget terms diagnosed from the emission-driven CH4E run are within the range of estimates from bottom-up studies as reported by Saunois et al. (2025). The CH4E simulations show a higher surface uptake than in the standard prescribed concentration run (35.7 vs. 34.2 Tg/yr), reflecting the zonal asymmetry associated with higher $CH_4$ over continental regions. The stratospheric loss term is similar for the two runs (35.7 Tg/yr in STD, 35.6 Tg/yr in

https://doi.org/10.5194/egusphere-2026-5718
Preprint. Discussion started: 15 October 2026
© Author(s) 2026. CC BY 4.0 License.

CH4E), both within the range of estimates from other recent studies.

**Table 3.** $CH_4$ budgets (Tg/yr) and lifetime (years) from 2000 to 2017

| | Period | Emission | Chem loss (OH) | Surface uptake | Strat Loss | Burden | Total lifetime[4] | Lifetime due to OH loss |
|---|---|---|---|---|---|---|---|---|
| CMIP6[1] | 2000-2009 | 638[3] | 541 | 30 | 39 | / | 8.2 | 9.3[5] |
| CMIP6[1] | 2010-2019 | 669[3] | 563 | 31 | 37 | / | 8.2 | 9.2[5] |
| UKESM1-ems[2] | 2000-2009 | 591 | 525 | 31 | 23 | / | / | 8.5±0.1 |
| STD_Fix | 2000-2009 | / | 504 | 33.8 | / | 5042 | / | 9.95 |
| STD_Fix | 2010-2017 | / | 519 | 34.6 | / | 5163 | / | 9.90 |
| STD | 2000-2009 | / | 503 | 33.8 | 35.7 | 4946 | 8.64 | 9.78 |
| STD | 2010-2017 | / | 518 | 34.6 | 35.6 | 5049 | 8.58 | 9.70 |
| CH4E | 2000-2009 | 590 | 506 | 35.1 | 35.0 | 4955 | 8.60 | 9.74 |
| CH4E | 2010-2017 | 617 | 524 | 36.2 | 36.1 | 5127 | 8.60 | 9.74 |

[1]mean values, Saunois et al. (2025)
[2]Folberth et al. (2022)
[3]bottom-up, Saunois et al. (2025)
[4]defined as total burden divided by total loss which includes tropospheric chemical loss, stratospheric removal, and surface uptake to soils.
[5]tropospheric lifetime defined as total burden divided by tropospheric loss.

The $CH_4$ total lifetime and lifetime due to OH loss are shown in **Table 3**. The total lifetime is calculated as the global $CH_4$ burden divided by the total sink where the latter includes removal of $CH_4$ by oxidation in the troposphere, stratospheric removal, and surface uptake to soils. The total $CH_4$ lifetime from the emission-driven and prescribed concentration runs are similar (~8.6 years), indicating that there is little sensitivity to the approach used to implement $CH_4$ in the model. The chemical lifetime due to OH loss is also similar (~9.7 years) but is notably shorter than for the STD_Fix run (9.9 years) where uniform mixing ratios are prescribed throughout the depth of the troposphere. This highlights the importance of representing the vertical profile of $CH_4$ appropriately.

### 3.3 Differences in $CH_4$ spatial and temporal distribution

The impact of incorporating $CH_4$ emissions in the CH4E simulation is clearly apparent in the simulated global surface distribution of $CH_4$, as expected. (**Figure 5**). Enhanced $CH_4$ concentrations in the emission-driven simulation are observed in regions with significant anthropogenic emissions, including the USA, Europe, India, East Asia and Southeast Asia. Additionally, natural sources, such as wetland emissions, contribute to higher $CH_4$ concentrations in areas such as Central Africa. Biomass burning also contributes to high $CH_4$ concentrations over Central Africa. In the Arctic, higher levels of $CH_4$ are simulated in the CH4E run due to transport from lower latitudes, particularly from sources over Eurasia (Liu et al., 2025).

The two prescribed-concentration simulations (STD_Fix and STD) have the same prescribed surface $CH_4$ distribution, but differ in their vertical distribution: $CH_4$ is prescribed throughout the atmosphere in STD_Fix, but only at the surface in STD. Consequently, STD develops a vertical $CH_4$ gradient

https://doi.org/10.5194/egusphere-2026-5718
Preprint. Discussion started: 15 October 2026
© Author(s) 2026. CC BY 4.0 License.

through atmospheric transport and chemical loss, similar to that in the emission-driven CH4E simulation (**Figure 5c, d**). Both STD and CH4E show a gradual decrease in $CH_4$ from the surface to the tropopause, with broadly similar vertical gradients, particularly in the northern mid- and high latitudes where $CH_4$ abundances are highest. $CH_4$ concentrations are generally higher in CH4E than in STD, reflecting differences arising from the explicit treatment of surface emissions and atmospheric sinks. Overall, the emission-driven treatment has a relatively small effect on the large-scale vertical gradient of $CH_4$, which is primarily controlled by atmospheric transport and chemical loss, although regional differences can arise from the spatial distribution of emissions and their interaction with transport.

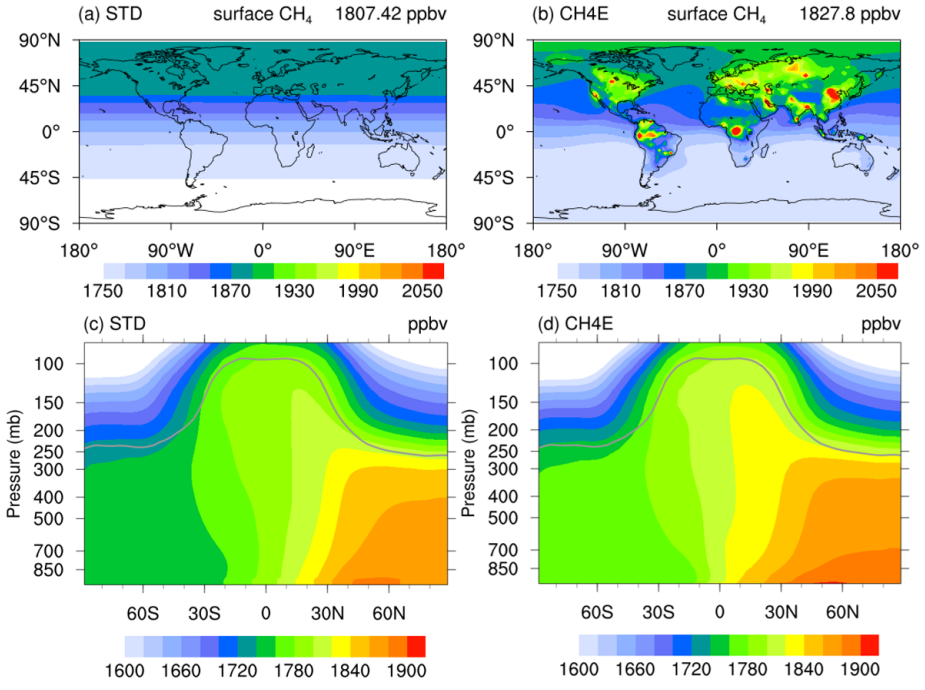


**Figure 5.** Multi-year averaged annual surface distributions and vertical profiles of $CH_4$ mixing ratio (ppbv) from 2000 to 2017, derived from (a, c) STD and (b, d) CH4E simulations. Values in the upper right corner of the surface panels represent the global mean concentrations. The grey line in the vertical panels indicates the tropopause, defined by a 150 ppbv $O_3$ concentration.

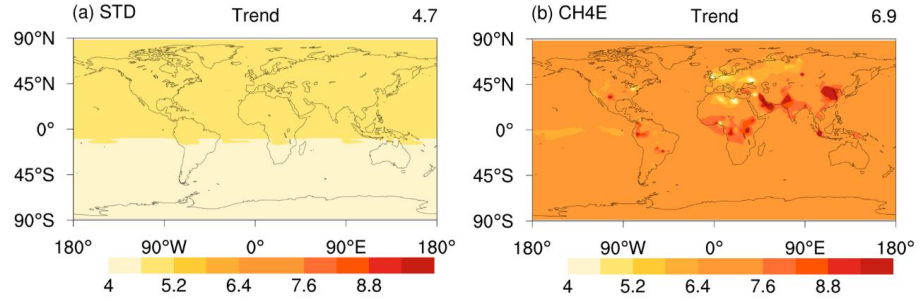


**Figure 6.** Spatial distribution of annual trends in surface $CH_4$ during 2000–2017 (ppbv·yr$^{-1}$) in the (a) STD and (b) CH4E model runs. Trends were derived using the Theil–Sen estimator. Statistically significant trends at the

https://doi.org/10.5194/egusphere-2026-5718
Preprint. Discussion started: 15 October 2026
© Author(s) 2026. CC BY 4.0 License.

95% confidence level were assessed using the Mann-Kendall test. The trends are statistically significant across the entire global dataset. The value in the upper right corner of each panel represents the global mean trend in ppbv·yr$^{-1}$.

In comparing concentration and emission-driven approaches to implementing $CH_4$, another key issue is if and how long-term trends differ on a regional basis. The growth rate of atmospheric $CH_4$ in the prescribed concentration simulation is 4.7 ppbv·yr$^{-1}$ (**Figure 6a**), consistent with the NOAA GML observations, which show a linear increase of 4.58 ± 0.39 ppbv·yr$^{-1}$ during 2000–2017 (Lan et al., 2026). From **Figure 6**, clear differences in the simulated $CH_4$ trend are apparent between the prescribed concentration and emission-driven runs, with the latter exhibiting much greater spatial structure. Stronger positive trends are observed in regions such as Africa, South America, India, East Asia and Southeast Asia. For example, $CH_4$ trends exceed 10 ppbv·yr$^{-1}$ over northern China, while remaining below 4 ppbv·yr$^{-1}$ over Europe, indicating a more than twofold difference between these regions. These enhanced trends are likely driven by significant increases in $CH_4$ emissions in these areas and reflect an improved sensitivity to regional emission sources and their impact on global $CH_4$ concentrations and trends in the emission-driven run.

### 3.4 Impact on tropospheric $O_3$ and OH

The tropospheric $O_3$ and OH budget from the different runs are summarized in **Table 4**. In the emission-driven CH4E run, the tropospheric $O_3$ burden is ~2.0 Tg (0.6%) larger than in the prescribed concentration STD run, and the OH burden is 0.1 Mg (0.05%) larger. Despite the higher $O_3$ burden, the tropospheric $O_3$ lifetime remains largely unchanged. The sensitivity of the $O_3$ and OH global budget terms to the approach to implementing $CH_4$ is thus very small. In STD_Fix, where concentrations are prescribed uniformly in altitude, the $O_3$ burden is almost the same as in STD, where concentrations are prescribed at the surface only, but OH is lower due to greater OH reaction with $CH_4$ due to the higher $CH_4$ abundance in the upper troposphere.

**Table 4.** Tropospheric budgets of $O_3$ and OH and atmosphere lifetime (days) in the model averaged over the 2000-2017 period.

| | | $O_3$ (Tg·yr$^{-1}$) | | | Trop OH | $[OH]_{gm}$ |
|---|---|---|---|---|---|---|
| | Lifetime | Burden (Tg) | Prod | Loss | Burden (Mg) | (Molecules·cm$^{-3}$) |
| STD_Fix | 29.1 | 348.4 | 5077 | 4379 | 208.7 | 10.86 |
| STD | 29.1 | 348.3 | 5074 | 4376 | 209.0 | 10.88 |
| CH4E | 29.1 | 350.1 | 5102 | 4400 | 209.1 | 10.88 |

In CH4E, the higher $O_3$ burden is mainly driven by elevated $CH_4$ levels, which serve as a key precursor for $O_3$ formation through oxidation processes. Enhanced $CH_4$ oxidation promotes $O_3$ production, as reflected in the production terms shown in **Table 4**. As one of the primary sources of OH is via the photolysis of $O_3$ (for a chemical budget analysis, see **Table S3**), the higher $O_3$ concentration under CH4E contributes to increased OH production. However, $CH_4$ is also a major sink for OH, and the enhanced $CH_4$ levels lead to increased OH consumption through oxidation. As a result, the net increase in OH is small due to the competing effects of $O_3$-driven production and $CH_4$-driven loss. These results highlight the complex and nonlinear interactions between $CH_4$, $O_3$, and OH radicals in the troposphere, and emphasize the importance of considering both source and

https://doi.org/10.5194/egusphere-2026-5718
Preprint. Discussion started: 15 October 2026
© Author(s) 2026. CC BY 4.0 License.

sink processes in evaluating atmospheric oxidant budgets.

The surface and zonal mean $O_3$ distributions from the STD run and the differences between CH4E and STD runs are shown in **Figure 7**. The distributions for the STD_Fix run are similar to those from STD and are not shown here. At the surface, the STD run exhibits the expected inhomogeneous distribution, with annual mean surface $O_3$ generally higher in the northern hemisphere than in the southern hemisphere, with mixing ratios peaking at approximately 60 ppbv over the Tibetan Plateau (**Figure 7a**). Higher surface $O_3$ is simulated in the CH4E run over much of the world but the differences are small (globally averaged, +0.2ppbv; **Figure 7b**). In regions such as East Asia and parts of Europe and North America, larger surface $O_3$ increases of 0.3 ppbv are apparent due to higher $CH_4$ concentrations and more efficient $O_3$ production in VOCs-sensitive regions (Liu et al., 2022). In the vertical, the CH4E run shows a similar structure but exhibits slightly higher $O_3$ concentrations at higher latitude (**Figure 7c and 7d**), where differences reach 0.4 ppbv in the mid- and upper-troposphere.

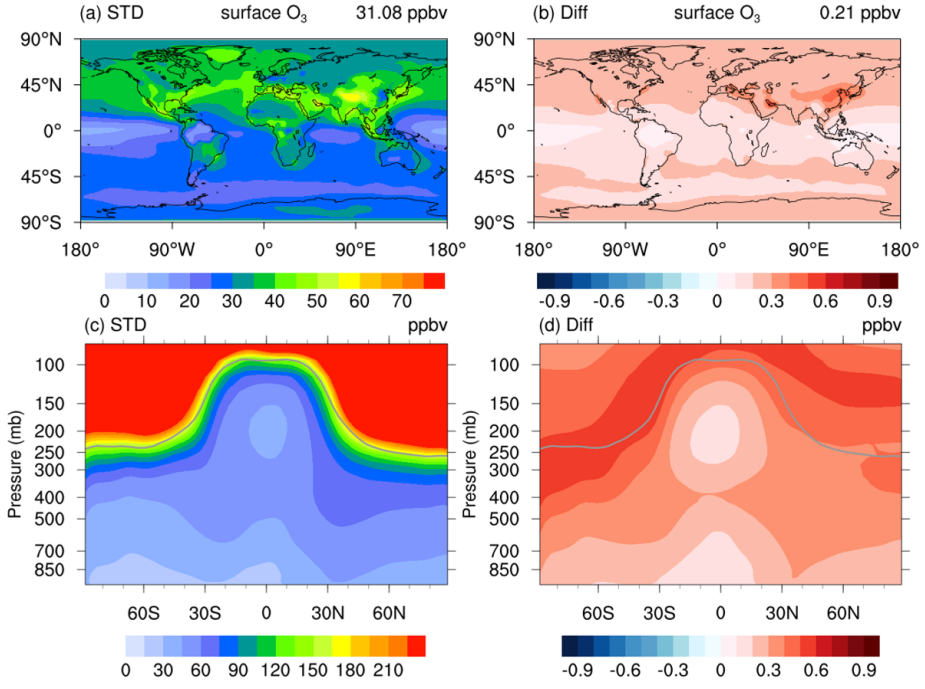


**Figure 7.** (a, c) Multi-year averaged annual surface $O_3$ mixing ratio (ppbv) and latitude-pressure $O_3$ distribution (ppbv) from 2000 to 2017, based on the STD simulation. (b, d) Corresponding differences between the CH4E and STD simulations. The values in the upper right corner of the surface $O_3$ panels indicate the global mean mixing ratios. The grey line in the vertical distribution panels marks the tropopause, defined by an $O_3$ mixing ratio of 150 ppbv.

https://doi.org/10.5194/egusphere-2026-5718
Preprint. Discussion started: 15 October 2026
© Author(s) 2026. CC BY 4.0 License.

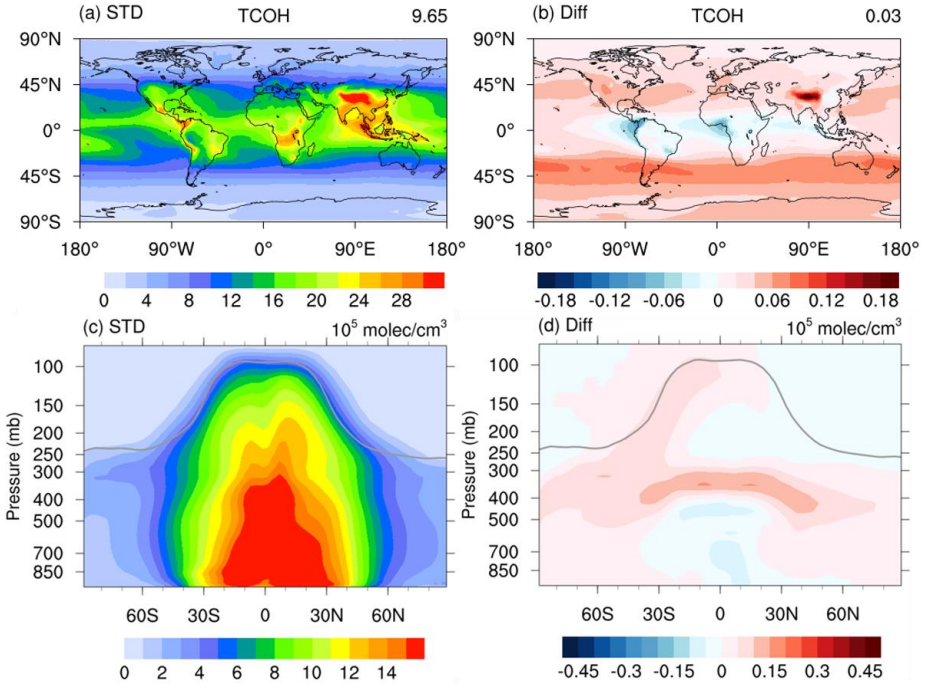


**Figure 8.** As Figure 7, but for annual tropospheric OH column (TCOH, $10^{12}$ molecules·cm$^{-2}$) and [OH] vertical distribution ($10^5$ molecules·cm$^{-3}$).

The global distribution of the tropospheric OH column (TCOH) and the zonal mean OH concentrations averaged over 2000–2017 are shown in **Figure 8**. In the STD run, the OH column exhibits a pronounced spatial pattern, with elevated values primarily located in tropical and subtropical regions such as Southeast Asia, central Africa, and northern South America. These regions coincide with strong solar radiation and high humidity, which favor $O_3$ photolysis and subsequent OH formation. The global mean OH column is $9.65 \times 10^{12}$ molecules·cm$^{-2}$.

The differences in tropospheric OH column associated with the emissions-driven CH4E run are relatively small ($+0.03\times10^{12}$ molecules·cm$^{-2}$), but clear regional differences are observed. Small positive anomalies are found in East and Southeast Asia and over the mid-latitude oceans, while negative anomalies appear over tropical regions, such as South America and Africa. These patterns reflect the dual role of $CH_4$ in enhancing $O_3$ formation, which promotes OH production via photolysis, but acting as a direct sink of OH through oxidation. The net effect on OH depends on the local balance of these processes.

The zonal mean vertical distribution further reveals that OH concentrations peak in the tropical troposphere (surface to 250 mb), consistent with strong photochemical activity in this region. Under the CH4E run, OH concentrations are slightly higher by up to $0.2 \times 10^5$ molecules·cm$^{-3}$ in the middle troposphere, especially in the tropics where $CH_4$ contributes to $O_3$ and subsequent OH production. In contrast, at lower altitudes, tropical and northern hemisphere regions show minor OH reductions due to increased consumption by $CH_4$ oxidation. Overall, these results highlight the subtle but non-negligible impact of $CH_4$ on tropospheric OH, with altitude- and region-dependent effects governed

https://doi.org/10.5194/egusphere-2026-5718
Preprint. Discussion started: 15 October 2026
© Author(s) 2026. CC BY 4.0 License.

by the interplay between OH sources and sinks.

### 3.5 Impact on OH and $O_3$ trends

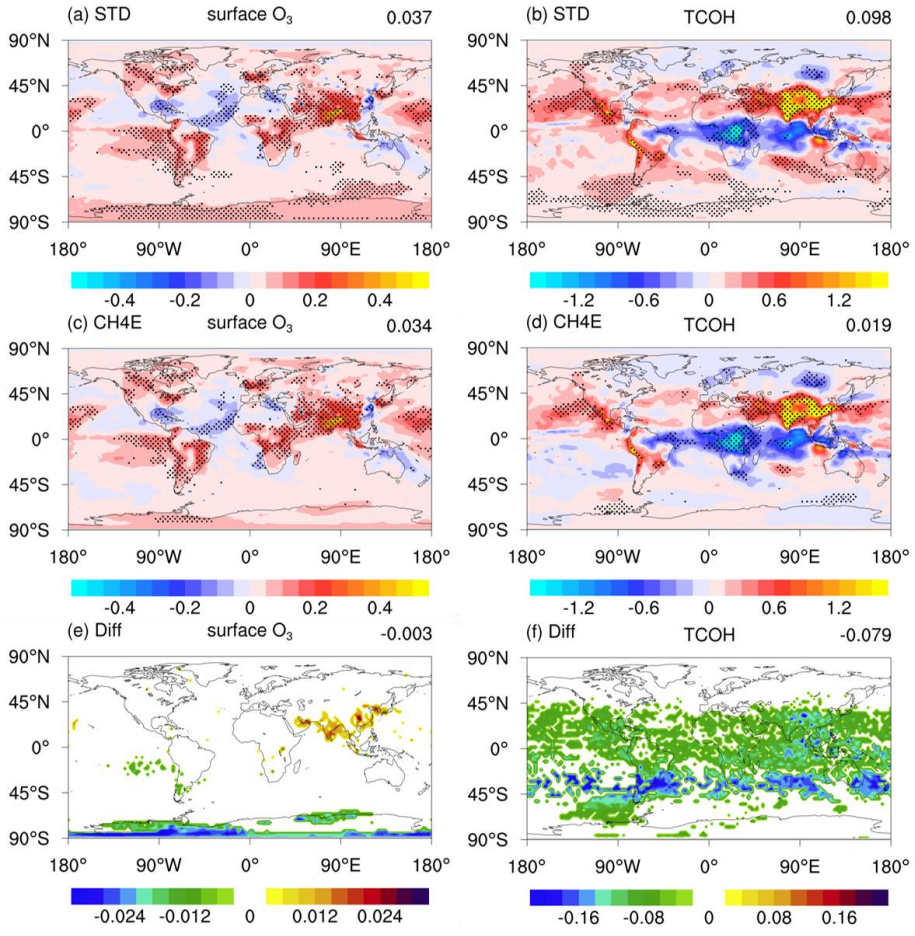


**Figure 9.** Spatial distribution of annual trends in surface $O_3$ (ppbv·yr$^{-1}$, a and c) and tropospheric column OH ($10^{11}$ molecules·cm$^{-2}$·yr$^{-1}$, b and d). Panels (e) and (f) show the differences in trends between CH4E and STD.

In the prescribed concentration STD simulation, surface $O_3$ shows small positive trends, especially in Europe, North America, South America, and South Asia (see **Figure 9**). The emission-driven CH4E run shows similar trends but with slightly larger $O_3$ increases (~10%) in South and East Asia and smaller $O_3$ increases at southern high latitudes. The higher $O_3$ increase in South and East Asia is primarily driven by the high $NO_x$ abundance in these regions, where higher $CH_4$ concentrations enhance the efficiency of $O_3$ formation.

For OH, the STD simulation produces a larger positive trend in the troposphere, particularly in the tropics and northern hemisphere. The CH4E run shows a slower increase in OH column, particularly in the tropics and Southern Hemisphere mid-latitudes. This is because higher $CH_4$ in the CH4E simulation leads to higher $CH_4$ oxidation, consuming more OH, and reduces the overall OH column growth relative to the STD simulation. In the Southern Hemisphere, TCOH shows a smaller increase

https://doi.org/10.5194/egusphere-2026-5718
Preprint. Discussion started: 15 October 2026
© Author(s) 2026. CC BY 4.0 License.

or even a small decrease that may be associated with the slower $O_3$ growth in this region.

### 3.6 Influence of $CH_4$ treatment on its chemical feedback

Understanding the feedback of $CH_4$ on its own lifetime is essential for quantifying the response of atmospheric $CH_4$ to perturbations in its sources and sinks, and plays a critical role in assessing future climate forcing. In this study, we calculate the feedback factor (F) for each of the three approaches we have used to implement $CH_4$, following the methods described in Holmes (2018). For each approach we perform an additional simulation where the prescribed concentration (for STD and STD_Fix) or emission (for CH4E) is increased by 20%, and we focus on the responses in the year 2010. We use a 2.5-year spin-up for the prescribed concentration everywhere (STD_Fix) and 14.5-year spin-up for the prescribed concentration at surface (STD) and emissions-driven simulation (CH4E). We calculate two feedback factors: a conventional feedback factor based on the derived chemical loss to OH and recommended lifetimes for other sinks (stratosphere: 120 years, deposition: 150 years, Cl loss: 200 years) following Prather et al. (2012), and a model feedback factor based on the sinks diagnosed in the model only. The conventional feedback factor permits direct comparison with previous studies, while the model feedback factor characterizes the true behavior of $CH_4$ in the simulations performed here.

**Table 5**. $CH_4$ budget terms and feedback factors simulated with the prescribed and emission-driven $CH_4$ configurations

| | STD_Fix | STD | CH4E |
|---|---|---|---|
| Chemical lifetime (years) | 9.93 | 9.73 | 9.82 |
| Total lifetime (years) | 8.75 | 8.59 | 8.62 |
| $CH_4$ burden 2010 (Tg) | 5013 | 4999 | 5144 |
| $CH_4$ burden change (Tg) | +1021 (20%) | +1000 (20%) | +1108 (22%) |
| Conventional feedback factor, $F_t$ | 1.4089 | 1.4094 | 1.4027 |
| Model feedback factor, F | 1.4422 | 1.4389 | 1.4394 |

As shown in **Table 5**, the 20% perturbation in atmospheric $CH_4$ concentrations in the prescribed concentration simulations resulted in increases in $CH_4$ burden of 1021 and 1000 Tg. In the emission-driven simulation, a 20% increase in $CH_4$ emissions produced a slightly larger relative increase in the $CH_4$ burden, reaching 1108 Tg (22%). Despite these differences, the calculated feedback factors were highly consistent among the three configurations. Using the conventional formulation with model-diagnosed $CH_4$ chemical loss by OH, together with recommended loss frequencies for Cl oxidation, stratospheric loss, and soil uptake, the feedback factors were 1.4089, 1.4094, and 1.4027 for STD_Fix, STD, and CH4E, respectively. The differences in the feedback factors among the three $CH_4$ configurations are therefore small, indicating that the approach to representing $CH_4$ has only a minor effect on the diagnosed feedback factor. This result is consistent with the findings of Holmes (2018). When the feedback factor was calculated using only the $CH_4$ loss processes diagnosed directly by the model, excluding Cl oxidation, the corresponding values were 1.4422, 1.4389, and 1.4394, which are slightly higher than those obtained using the conventional formulation. This difference suggests a stronger diagnosed $CH_4$ feedback when the model-simulated loss processes are used and highlights the sensitivity of the feedback factor to the treatment of individual $CH_4$ sinks, particularly neglect of Cl oxidation.

https://doi.org/10.5194/egusphere-2026-5718
Preprint. Discussion started: 15 October 2026
© Author(s) 2026. CC BY 4.0 License.

### 3.7 Response to surface NOx emissions

As well as acting as an important source of key oxidants such as ozone, NOx emissions have pronounced impacts on the atmospheric $CH_4$ burden through their influence on tropospheric OH (Wild et al., 2001; Derwent et al., 2001). To explore how the treatment of $CH_4$ influences assessment of the impacts of NOx emission changes, we conduct additional simulations with a 20% reduction in surface NO emissions applied in the first year only and follow the subsequent response. We do this for the prescribed surface concentration (STD) and emission-driven (CH4E) approaches, and perform additional emission-driven runs using repeating year 2000 precursor emissions and meteorology (CH4E_Fix) to investigate the effects of these factors on the response.

As shown in **Figure 10**, the NO emission reduction induces an immediate and short-lived decrease in $O_3$ and OH burdens of a similar magnitude in all runs, and these lead to a rapid increase in the $CH_4$ burden in the emissions-driven run that peaks at 21.5 Tg ($CH_4$) in 2001, the year after the NO emission reduction. This corresponds to an increase in surface $CH_4$ abundance of 5.0 ppbv, comparable in magnitude to the 4.8±1.0 ppbv increase seen over the COVID-19 lockdown period in 2020 diagnosed by Stevenson et al. (2022) that was associated with a ~15% NOx emission reduction. Thereafter, the $CH_4$ anomaly decays exponentially with a perturbation lifetime of 12.5 years, matching that expected for the CH4E simulation with a $CH_4$ total lifetime of 8.6 years and feedback factor F of 1.45, and similar to that found in previous studies (IPCC 1996; Prather 2007). We note that the decay of this perturbation is exponential and uniform after 2001, reflecting the principal natural mode in the tropospheric chemical scheme (Wild and Prather, 2000) and that it is largely unaffected by underlying changes in emissions or meteorology over the 2000-2017 period, as postulated by Holmes (2018). The impacts on $CH_4$ abundance are much smaller in the prescribed surface concentration (STD) run, as expected, but the changes in $O_3$ and OH persist over 2-3 years reflecting changes in short-lived chemical modes associated with CO-OH-$O_3$ interactions. In the emission-driven (CH4E) run, the initial $O_3$ decrease in the first year is replaced by an $O_3$ increase from 2002 associated with the higher $CH_4$ abundance, and this decays with the same timescale as the $CH_4$ anomaly. While these changes are small, 1-2% of the $O_3$ change seen under the emission pulse in 2000, the accumulated burden change over the lifetime of the anomaly is 3.1 Tg·yr$^{-1}$, which offsets one third of the 9.2 Tg $O_3$ increase seen in 2000. Model studies using prescribed $CH_4$ concentrations are unable to represent these responses without additional adjustment, and this highlights the importance of using an emission-driven approach for assessing long-term climate responses.

https://doi.org/10.5194/egusphere-2026-5718
Preprint. Discussion started: 15 October 2026
© Author(s) 2026. CC BY 4.0 License.

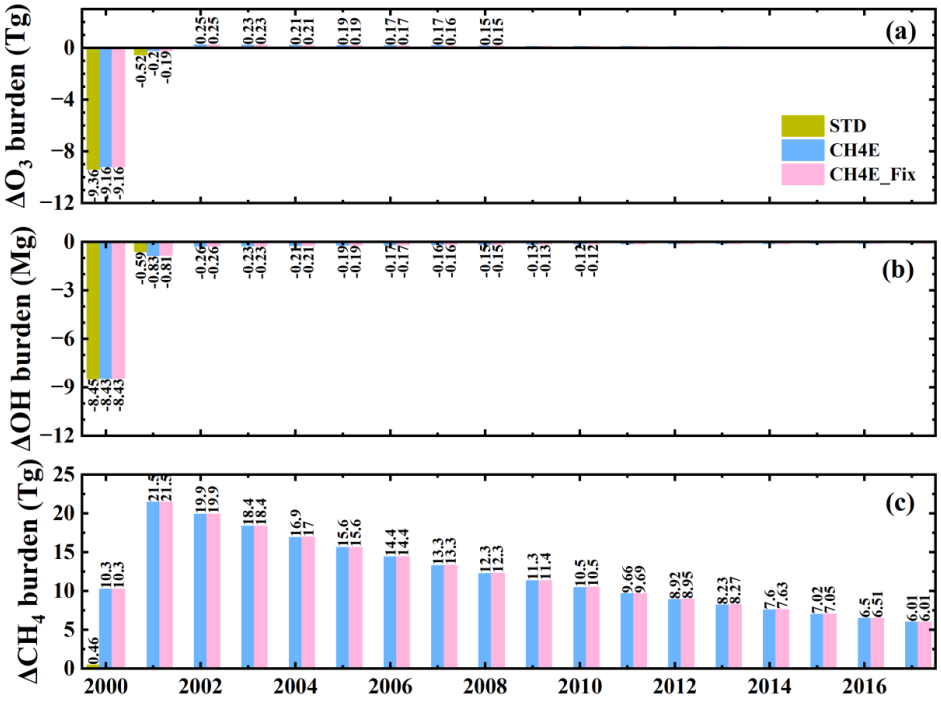


**Figure 10.** Temporal differences in (a) $O_3$ burden (Tg), (b) OH burden (Mg), and (c) $CH_4$ burden (Tg) from 2000 to 2017 in response to a 20 % reduction in NO surface emissions applied in year 2000 only. Results are shown for prescribed surface $CH_4$ concentration (STD) and emission-driven (CH4E) approaches, and for an emission-driven approach using repeating year 2000 precursor emissions and meteorology (CH4E_Fix).

## 4 Conclusions

A thorough assessment of how atmospheric $CH_4$ responds to its sources and sinks is essential for improving understanding of the $CH_4$ budget and advancing knowledge of air quality and anthropogenic climate change. In this study, we evaluated three treatments of $CH_4$ in a chemical transport model: prescribing mixing ratios throughout the troposphere, prescribing mixing ratios at the surface only, and incorporating a full treatment of $CH_4$ emissions. We investigated the impact of each approach on the simulated $CH_4$ budget and on how key tropospheric oxidants ($O_3$ and OH) respond to changing emissions and meteorology over the 2000-2017 period. We incorporate $CH_4$ emissions from anthropogenic, wetland, fires, geological, termite and biogenic sources which give a global $CH_4$ source of 602 Tg/yr over the 2000-2017 study period. We incorporate explicit treatments of surface uptake (averaging 35.6 Tg/yr), and stratospheric $CH_4$ loss (averaging 35.5 Tg/yr). The total atmospheric $CH_4$ lifetime in the emissions-driven simulation is 8.6 years, and the lifetime to chemical loss by reaction in the troposphere is 9.7 years. These modelled budget terms compare well with observation-based estimates from Saunois et al., (2025).

The emission-driven simulation successfully reproduces key features of the tropospheric $CH_4$ distribution seen in surface and aircraft $CH_4$ measurements, including the interhemispheric gradient, vertical distribution, seasonal variability, and long-term annual trends. As expected, it shows

https://doi.org/10.5194/egusphere-2026-5718
Preprint. Discussion started: 15 October 2026
© Author(s) 2026. CC BY 4.0 License.

substantially greater spatial variability in surface $CH_4$ than the prescribed concentration approaches, reflecting the spatial heterogeneity of source distributions. It also captures significantly stronger positive $CH_4$ trends in Africa, South America, India, and East and Southeast Asia, highlighting the importance of employing an emission-based framework to assess regional $CH_4$ trends.

The effect of different $CH_4$ treatments on tropospheric oxidants is relatively small. In the emissions-driven simulation surface $O_3$ is slightly higher globally due to the higher $CH_4$ levels, with the most pronounced increases (~0.4 ppbv) over East Asia, North America, and the southern hemisphere. The global tropospheric $O_3$ burden is 2.0 Tg (0.6%) larger than in the prescribed concentration simulation. Similarly, the OH burden is marginally (0.05%) greater. An increasing trend in surface $O_3$ is seen in all model runs, notably over Europe, North America, South America, East Asia and South Asia. However, the emission-driven simulation shows a slower $O_3$ growth rate at southern hemisphere high latitudes and a faster growth rate in South and East Asia under the influence of high regional NOx and VOCs concentrations. The emission-driven run shows a smaller positive trend in tropospheric OH due to enhanced OH consumption by $CH_4$ oxidation.

A 20% $CH_4$ perturbation results in a slightly larger increase in $CH_4$ burden in the emission-driven approach (~22%) than in the prescribed-concentration approaches (~20%). The conventional $CH_4$ feedback factors, which combine model-diagnosed OH loss with recommended lifetimes for other $CH_4$ sinks (Prather et al., 2012), are highly consistent across the different approaches (1.403–1.409), demonstrating that the simulated $CH_4$–OH feedback is largely insensitive to the choice of approach taken. Feedback factors derived from model-diagnosed $CH_4$ sinks are slightly higher (~1.440), indicating sensitivity to the representation of $CH_4$ loss processes.

The treatments of $CH_4$ have pronounced influences on the long-term response to changes in NOx emissions. A 20% reduction in surface NO emissions produces similar immediate decreases in OH and $O_3$ across the different $CH_4$ treatments, but the emission-driven simulation additionally captures a persistent $CH_4$ perturbation, with a peak burden increase of 21.5 Tg in the year following the perturbation and subsequently decaying with a perturbation lifetime of 12.5 years. This long-term $CH_4$ response is largely unaffected by interannual variations in meteorology and emissions of $CH_4$ and other species. The resulting increase in $CH_4$ subsequently enhances $O_3$, partially offsetting the initial $O_3$ decrease. These longer-lived $CH_4$–$O_3$ responses are not fully represented when $CH_4$ concentrations are prescribed, highlighting the importance of an emission-driven treatment of $CH_4$ for assessing the longer-term atmospheric response to emission perturbations.

In summary, the updates to the FRSGC/UCI chemical transport model described here offer new capability and we have demonstrated that the model is capable of simulating $CH_4$ well when using emissions. While prescribed $CH_4$ concentrations may be sufficient for many studies of tropospheric composition, an emission-driven treatment is important for capturing longer-term $CH_4$–OH–$O_3$ responses to changes in emissions. This capability therefore provides a more complete framework for investigating the impacts of future emission changes on atmospheric chemistry and climate.

**Data availability.** The model output from the simulations described in this work are available on Zenodo (Hou et al., 2026; https://zenodo.org/uploads/22030169). $CH_4$ measurements from the NOAA Global Monitoring Laboratory network are publicly available at https://gml.noaa.gov/ccgg/data/getdata.php?gas=ch4 (last access: 19 August 2026). Anthropogenic $CH_4$ emissions from the CMIP7 input4MIPs historical forcing dataset are available through ESGF at

https://doi.org/10.5194/egusphere-2026-5718
Preprint. Discussion started: 15 October 2026
© Author(s) 2026. CC BY 4.0 License.

https://esgf-node.ornl.gov/search/input4mips/ (last access: 19 August 2026). Wetland emissions from the WetCHARTs v1.0 extended ensemble are available at https://doi.org/10.3334/ORNLDAAC/1502. Fire emissions from GFED4s are available at https://www.globalfiredata.org/ (last access: 19 August 2026). Biogenic $CH_4$ emissions from CAMS-GLOB-BIO v3.1 and termite emissions from CAMS-GLOB-TERM v1.1 are available through the Copernicus Atmosphere Data Store at https://ads.atmosphere.copernicus.eu/datasets/cams-global-emission-inventories (last access: 19 August 2026). Geological $CH_4$ emissions from the Global Carbon Project Methane Budget 2024 dataset are available at https://doi.org/10.18160/GKQ9-2RHT (Martinez et al., 2024).

**Author contributions.** XH and RH designed the study and updated the emission inventories. XH and OW updated the model code. XH conducted the modeling and data analysis with contributions from RH, OW, JL, and YW. JL and YW discussed the results and offered valuable comments. XH, RH and OW wrote the paper with input from all authors.

**Competing interests.** The authors declare that they have no conflict of interest.

**Acknowledgements.** We acknowledge the High-End Computing (HEC) high-performance and high-throughput computing facilities at Lancaster University, UK, and the High-Performance Computing Center of Nanjing University of Information Science and Technology, China, for providing the computational resources used in this study. We are grateful to the providers of the $CH_4$ emission inventories and observational datasets for making these data publicly available. We also thank Gerd Folberth from the UK Met Office Hadley Centre for his valuable advice on the setup and implementation of the methane emissions-driven simulation.

**Financial support.** This research was supported by the National Key Research and Development Program of China (grant no. 2022YFC3701204 and 2023YFC3709405), and NERC grants LSO3 (NE/V011863/1) and InHALE (NE/X003582/).

## References

Bloom, A. A., Bowman, K. W., Lee, M., Turner, A. J., Schroeder, R., Worden, J. R., Weidner, R., McDonald, K. C., and Jacob, D. J.: A global wetland methane emissions and uncertainty dataset for atmospheric chemical transport models (WetCHARTs version 1.0), Geosci. Model Dev., 10, 2141–2156, https://doi.org/10.5194/gmd-10-2141-2017, 2017.

Brown, A. T., Volk, C. M., Schoeberl, M. R., Boone, C. D., and Bernath, P. F.: Stratospheric lifetimes of CFC-12, CCl4, CH4, CH3Cl and N2O from measurements made by the Atmospheric Chemistry Experiment-Fourier Transform Spectrometer (ACE-FTS), Atmos. Chem. Phys., 13, 6921–6950, https://doi.org/10.5194/acp-13-6921-2013, 2013.

Burkholder, J. B., Sander, S. P., Abbatt, J., Barker, J. R., Cappa, C., Crounse, J. D., Dibble, T. S., Huie, R. E., Kolb, C. E., Kurylo, M. J., Orkin, V. L., Percival, C. J., Wilmouth, D. M., and Wine, P. H.: Chemical Kinetics and Photochemical Data for Use in Atmospheric Studies, Evaluation No. 19, JPL Publication 19-5, Jet Propulsion Laboratory, Pasadena, https://dataverse.jpl.nasa.gov/file.xhtml?fileId=54539&version=2.1 (last access: 28 September 2026), 2020.

Derwent, R. G., Collins, W. J., Johnson, C. E., and Stevenson, D. S.: Transient Behaviour of Tropospheric Ozone Precursors in a Global 3-D CTM and Their Indirect Greenhouse Effects, Clim. Change, 49, 463–

https://doi.org/10.5194/egusphere-2026-5718
Preprint. Discussion started: 15 October 2026
© Author(s) 2026. CC BY 4.0 License.



487, https://doi.org/10.1023/A:1010648913655, 2001.

Dlugokencky Edward J., Nisbet Euan G..Fisher Rebecca and Lowry David: Global atmospheric methane: budget, changes and, dangers. Phil. Trans. R. Soc. A. 369: 2058-2072, http://doi.org/10.1098/rsta.2010.0341, 2011.

Dutaur L. and Verchot L. V.: A global inventory of the soil CH4 sink. Global Biogeochemical Cycles, 21, GB4013, doi:10.1029/2006GB002734, 2007.

Fiore, A. M., Dentener, F. J., Wild, O., Cuvelier, C., Schultz, M. G., Hess, P., Textor, C., Schulz, M., Doherty, R. M., Horowitz, L. W., MacKenzie, A., Sanderson, M. G., Shindell, D. T., Stevenson, D. S., Szopa, S., Van Dingenen, R., Zeng, G., Atherton, C., Bergmann, D., Bey, I., Carmichael, G., Collins, W. J., Duncan, B. N., Faluvegi, G., Folberth, G., Gauss, M., Gong, S., Hauglustaine, D., Holloway, T., Isaksen, I. S. A., Jacob, D. J., Jonson, J. E., Kaminski, J. W., Keating, T. J., Lupu, A., Marmer, E., Montanaro, V., Park, R. J., Pitari, G., Pringle, K. J., Pyle, J. A., Schroeder, S., Vivanco, M. G., Wind, P., Wojcik, G., Wu, S., and Zuber, A.: Multimodel estimates of intercontinental source-receptor relationships for ozone pollution, J. Geophys. Res.-Atmos., 114, D04301, doi:10.1029/2008JD010816, 2009.

Folberth, G. A., Staniaszek, Z., Archibald, A. T., Gedney, N., Griffiths, P. T., Jones, C. D., O'Connor, F. M., Parker, R. J., Sellar, A. A., Wiltshire A.: Description and evaluation of an emission-driven and fully coupled methane cycle in UKESM1. J. Adv. Model. Earth Syst., 14, e2021MS002982. https://doi.org/10.1029/2021MS002982, 2022.

Granier, C., S. Darras, H. Denier van der Gon, J. Doubalova, N. Elguindi, B. Galle, M. Gauss, M. Guevara, J.-P. Jalkanen, J. Kuenen, C. Liousse, B. Quack, D. Simpson, K. Sindelarova: The Copernicus Atmosphere Monitoring Service global and regional emissions (April 2019 version), Report April 2019 version, https://doi.org/10.24380/d0bn-kx16, 2019.

Granier, C., Guenther, A., Lamarque, J., Mieville, A., Muller, J., Olivier, J., Orlando, J., Peters, J., Petron, G., Tyndall, G., et al.: POET, a database of surface emissions of ozone precursors available online at: https://web.archive.org/web/20250204100902/http://accent.aero.jussieu.fr/database_table_inventories.php (last access: 28 September 2026), 2005.

Griffiths, P. T., Murray, L. T., Zeng, G., Shin, Y. M., Abraham, N. L., Archibald, A. T., Deushi, M., Emmons, L. K., Galbally, I. E., Hassler, B., Horowitz, L. W., Keeble, J., Liu, J., Moeini, O., Naik, V., O'Connor, F. M., Oshima, N., Tarasick, D., Tilmes, S., Turnock, S. T., Wild, O., Young, P. J., and Zanis, P.: Tropospheric ozone in CMIP6 simulations, Atmos. Chem. Phys., 21, 4187–4218, https://doi.org/10.5194/acp-21-4187-2021, 2021.

Hoesly, R., Smith, S., Ahsan, H., Prime, N., O'Rourke, P., Crippa, M., Klimont, Z., Guizzardi, D., Feng, L., Harkins, C., Mcdonald, B., Wang, S.: CEDS v_2025_04_18 Gridded Emissions Data 0.5 degree, zanodo, https://zenodo.org/records/15127477, 2025.

Holmes, C. D.: Methane feedback on atmospheric chemistry: Methods, models, and mechanisms, J. Adv. Model. Earth Syst., 10, 1087–1099, https://doi.org/10.1002/2017MS001196, 2018.

Holmes, C. D., Prather, M. J., Søvde, O. A., and Myhre, G.: Future methane, hydroxyl, and their uncertainties: key climate and emission parameters for future predictions, Atmos. Chem. Phys., 13, 285–302, https://doi.org/10.5194/acp-13-285-2013, 2013.

Hou, X.: model outputs for "Evaluation of emission-driven methane simulation and sensitivity of key atmospheric tracers to methane Representations" [Data set]. Zenodo. https://doi.org/10.5281/zenodo.22030169, 2026.

Hou, X., Hossaini, R., Wild, O., Mazzeo, A., Pope, R. J., Wang, Y., Wang, S., Zhao, Y., Lee, J., Zhu, B., Zhao, T., and Pandey, A. K.: Quantifying Drivers of Tropospheric OH and Its Trends: Sensitivity to Atmospheric Processes and Implications for Methane Lifetime, EGUsphere [preprint], https://doi.org/10.5194/egusphere-2026-3114, 2026.

IPCC: Climate Change 1995: The Science of Climate Change, Contribution of Working Group I to the Second Assessment Report of the Intergovernmental Panel on Climate Change, edited by Houghton, J. T., Meira Filho, L. G., Callander, B. A., Harris, N., Kattenberg, A., and Maskell, K., Cambridge University Press, Cambridge, UK, 94 pp., https://www.ipcc.ch/site/assets/uploads/2018/02/ipcc_sar_wg_I_full_report.pdf

https://doi.org/10.5194/egusphere-2026-5718
Preprint. Discussion started: 15 October 2026
© Author(s) 2026. CC BY 4.0 License.



(last access: 28 September 2026), 1996.

Jackson, R., Saunois, M., Bousquet, P., Canadell, J.G., Poulter, B., Stavert, A., Bergamaschi, P., Niwa, Y., Segers, A. and Tsuruta, A., Increasing anthropogenic methane emissions arise equally from agricultural and fossil fuel sources, Environ. Res. Lett, 15, 071002, doi:10.1088/1748-9326/ab9ed2, 2020.

Jacob, D. J., Varon, D. J., Cusworth, D. H., Dennison, P. E., Frankenberg, C., Gautam, R., Guanter, L., Kelley, J., McKeever, J., Ott, L. E., Poulter, B., Qu, Z., Thorpe, A. K., Worden, J. R., and Duren, R. M.: Quantifying methane emissions from the global scale down to point sources using satellite observations of atmospheric methane, Atmos. Chem. Phys., 22, 9617–9646, https://doi.org/10.5194/acp-22-9617-2022, 2022.

Kirschke, S., Bousquet, P., Ciais, P., Saunois, M., Canadell, J. G., Dlugokencky, E. J., Bergamaschi, P., Bergmann, D., Blake, D. R., Bruhwiler, L., Cameron-Smith, P., Castaldi, S., Chevallier, F., Feng, L., Fraser, A., Heimann, M., Hodson, E. L., Houweling, S., Josse, B., Fraser, P. J., Krummel, P. B., Lamarque, J.-F., Langenfelds, R. L., Le Quere, C., Naik, V., O'Doherty, S., Palmer, P. I., Pison, I., Plummer, D., Poulter, B., Prinn, R. G., Rigby, M., Ringeval, B., Santini, M., Schmidt, M., Shindell, D. T., Simpson, I. J., Spahni, R., Steele, L. P., Strode, S. A., Sudo, K., Szopa, S., van der Werf, G. R., Voulgarakis, A., van Weele, M., Weiss, R. F., Williams, J. E., and Zeng, G.: Three decades of global methane sources and sinks, Nat. Geosci., 6, 813–823, https://doi.org/10.1038/ngeo1955, 2013.

Lan, X., Petron, G., Baugh, K., Crotwell, A.M., Crotwell, M.J., DeVogel, S., Madronich, M., Mauss, J., Mefford, T., Moglia, E., Morris, S., Mund, J.W., Searle, A., Thoning, K.W., Wolter, S. and Miller, J.: Atmospheric Methane Dry Air Mole Fractions from the NOAA GML Global Greenhouse Gas Reference Network, Carbon Cycle Cooperative Global Air Sampling Network: 1983 - Present , Version: 2025-08-15, https://doi.org/10.15138/VNCZ-M766, 2025.

Lan, X., Thoning, K. W., and Dlugokencky, E. J.: Trends in globally-averaged $CH_4$, $N_2O$, and $SF_6$ determined from NOAA Global Monitoring Laboratory measurements, Version 2026-08, https://doi.org/10.15138/P8XG-AA10, 2026.

Lin, X., Peng, S., Ciais, P. Hauglustaine, D., Lan, X., Liu, G., Ramonet, M., Xi, Y., Yin, Y., Zhang, Z., Bösch, H., Bousquet, P., Chevallier, F., Dong, B., Gerlein-Safdi, C., Halder, S., Parker, R. J., Poulter, B., Pu, T., Remaud, M., Runge, A., Saunois, M., Thompson, R. L., Yoshida, Y., Zheng, B.: Recent methane surges reveal heightened emissions from tropical inundated areas. Nat. Commun., 15, 10894, https://doi.org/10.1038/s41467-024-55266-y. 2024.

Liu, G., Shen, L., Ciais, P., Lin, X., Hauglustaine, D., Lan, X., Turner, A. J., Zhu, Y. & Peng, S.: Trends in the seasonal amplitude of atmospheric methane. Nature, 1-6, https://doi.org/10.1038/s41586-025-08900-8, 2025.

Liu, Z., Doherty, R. M., Wild, O., O'Connor, F. M., and Turnock, S. T.: Tropospheric ozone changes and ozone sensitivity from the present day to the future under shared socio-economic pathways, Atmos. Chem. Phys., 22, 1209–1227, https://doi.org/10.5194/acp-22-1209-2022, 2022.

Martinez, A., Saunois, M., Poulter, B., Zhen, Z., Raymond, P., Regnier, P., Canadell, J. G., Jackson, R. B., Patra, P. K., Bousquet, P., Ciais, P., Dlugokencky, E. J., Lan, X., Allen, G., Bastviken, D., Beerling, D. J., Belikov, D., Blake, D., Castaldi, S., Crippa, M., Deemer, B. R., Dennison, F., Etiope, G., Gedney, N., Höglund-Isaksson, L., Holgerson, M. A., Hopcroft, P. O., Hugelius, G., Ito, A., Jain, A. K., Janardanan, R., Johnson, M. S., Kleinen, T., Krummel, P. B., Lauerwald, R., Li, T., Liu, X., McDonald, K. C., Melton, J. R., Mühle, J., Müller, J., Murguia-Flores, F., Niwa, Y., Noce, S., Pan, S., Parker, R. J., Peng, C., Ramonet, M., Riley, W. J., Rocher-Ros, G., Rosentreter, J. A., Sasakawa, M., Segers, A., Smith, S. J., Stanley, E. H., Thanwerdas, J., Tian, H., Tsuruta, A., Tubiello, F. N., Weber, T. S., van der Werf, G. R., Worthy, D. E. J., Xi, Y., Yoshida, Y., Zhang, W., Zheng, B., Zhu, Q., Zhu, Q., and Zhuang, Q.: Supplemental data of the Global Carbon Project Methane Budget 2024 v1 [data set], Global Carbon Project, https://doi.org/10.18160/GKQ9-2RHT, 2024.

McKain, K., Sweeney, C., Baier, B., Baugh, K., Crotwell, A., Crotwell, M., Handley, P., Higgs, J., Kaiser, E., Madronich, M., Miller, J. B., Moglia, E., Morris, S., Mund, J., Newberger, T., Petron, G., Verbeke, B., Wolter, S., and NOAA Global Monitoring Laboratory: NOAA Global Greenhouse Gas Reference Network Flask-Air PFP sample measurements of $CO_2$, $CH_4$, CO, $N_2O$, $H_2$, $SF_6$ and isotopic ratios collected from aircraft vertical profiles [data set], version 2026-08-10, https://doi.org/10.15138/39HR-9N34, 2026.

Meinshausen, M., Vogel, E., Nauels, A., Lorbacher, K., Meinshausen, N., Etheridge, D. M., Fraser, P. J.,

https://doi.org/10.5194/egusphere-2026-5718
Preprint. Discussion started: 15 October 2026
© Author(s) 2026. CC BY 4.0 License.

Montzka, S. A., Rayner, P. J., Trudinger, C. M., Krummel, P. B., Beyerle, U., Canadell, J. G., Daniel, J. S., Enting, I. G., Law, R. M., Lunder, C. R., O'Doherty, S., Prinn, R. G., Reimann, S., Rubino, M., Velders, G. J. M., Vollmer, M. K., Wang, R. H. J., and Weiss, R.: Historical greenhouse gas concentrations for climate modelling (CMIP6), Geosci. Model Dev., 10, 2057–2116, https://doi.org/10.5194/gmd-10-2057-2017, 2017.

Murguia-Flores, F., Jaramillo, V. J., & Gallego-Sala, A.: Assessing methane emissions from tropical wetlands: Uncertainties from natural variability and drivers at the global scale. Global Biogeochemical Cycles, 37(9), e2022GB007601. https://doi.org/10.1029/2022GB007601, 2023.

Myhre, G., D. Shindell, F.-M. Bréon, W. Collins, J. Fuglestvedt, J. Huang, D. Koch, J.-F. Lamarque, D. Lee, B. Mendoza, T. Nakajima, A. Robock, G. Stephens, T. Takemura and H. Zhang: Anthropogenic and Natural Radiative Forcing. In: Climate Change 2013: The Physical Science Basis. Contribution of Working Group I to the Fifth Assessment Report of the Intergovernmental Panel on Climate Change [Stocker, T.F., D. Qin, G.-K. Plattner, M. Tignor, S.K. Allen, J. Boschung, A. Nauels, Y. Xia, V. Bex and P.M. Midgley (eds.)]. Cambridge University Press, Cambridge, United Kingdom and New York, NY, USA, (https://www.ipcc.ch/site/assets/uploads/2018/02/WG1AR5_Chapter08_FINAL.pdf, last access: 28 September 2026), 2013.

Nisbet, E. G., Manning, M. R., Dlugokencky, E. J., Fisher, R. E., Lowry, D., Michel, S. E., Myhre, C. L., Platt, S. M., Allen, G., Bousquet, P., Brownlow, R., Cain, M., France, J. L., Hermansen, O., Hossaini, R., Jones, A. E., Levin, I., Manning, A. C., Myhre, G., Pyle, J. A., Vaughn, B. H., Warwick, N. J., and White, J. W. C.: Very Strong Atmospheric Methane Growth in the 4 Years 2014–2017: Implications for the Paris Agreement, Global Biogeochem. Cy., 33, 318–342, https://doi.org/10.1029/2018gb006009, 2019.

Nisbet, E., Manning, M. R., Dlugokencky, E. J., Michel, S. E., Lan, X., Rockmann, T., Denier Van Der Gon, H., Schmitt, J., Palmer, P. I., Dyonisius, M. N., Oh, Y., Fisher, R., Lowry, D., France, J., White, J. W. C., Brailsford, G., & Bromley, T.: Atmospheric methane: Comparison between methane's record in 2006-2022 and during glacial terminations. Global Biogeochemical Cycles, 37(8), Article e2023GB007875, https://doi.org/10.1029/2023GB007875, 2023.

Patra, P. K., Houweling, S., Krol, M., Bousquet, P., Belikov, D., Bergmann, D., Bian, H., Cameron-Smith, P., Chipperfield, M. P., Corbin, K., Fortems-Cheiney, A., Fraser, A., Gloor, E., Hess, P., Ito, A., Kawa, S. R., Law, R. M., Loh, Z., Maksyutov, S., Meng, L., Palmer, P. I., Prinn, R. G., Rigby, M., Saito, R., and Wilson, C.: TransCom model simulations of CH4 and related species: linking transport, surface flux and chemical loss with CH4 variability in the troposphere and lower stratosphere, Atmos. Chem. Phys., 11, 12813–12837, https://doi.org/10.5194/acp-11-12813-2011, 2011.

Prather, M. J.: Lifetimes and time scales in atmospheric chemistry, Philos. Trans. R. Soc. A, 365, 1705–1726, https://doi.org/10.1098/rsta.2007.2040, 2007.

Prather, M. J., Holmes, C. D., and Hsu, J.: Reactive greenhouse gas scenarios: Systematic exploration of uncertainties and the role of atmospheric chemistry, Geophys. Res. Lett., 39, L09803, https://doi.org/10.1029/2012GL051440, 2012.

Qu, Z., Jacob, D. J., Shen, L., Lu, X., Zhang, Y., Scarpelli, T. R., Nesser, H., Sulprizio, M. P., Maasakkers, J. D., Bloom, A. A., Worden, J. R., Parker, R. J., and Delgado, A. L.: Global distribution of methane emissions: a comparative inverse analysis of observations from the TROPOMI and GOSAT satellite instruments, Atmos. Chem. Phys., 21, 14159–14175, https://doi.org/10.5194/acp-21-14159-2021, 2021.

Saunois, M., Martinez, A., Poulter, B., Zhang, Z., Raymond, P. A., Regnier, P., Canadell, J. G., Jackson, R. B., Patra, P. K., Bousquet, P., Ciais, P., Dlugokencky, E. J., Lan, X., Allen, G. H., Bastviken, D., Beerling, D. J., Belikov, D. A., Blake, D. R., Castaldi, S., Crippa, M., Deemer, B. R., Dennison, F., Etiope, G., Gedney, N., Höglund-Isaksson, L., Holgerson, M. A., Hopcroft, P. O., Hugelius, G., Ito, A., Jain, A. K., Janardanan, R., Johnson, M. S., Kleinen, T., Krummel, P. B., Lauerwald, R., Li, T., Liu, X., McDonald, K. C., Melton, J. R., Mühle, J., Müller, J., Murguia-Flores, F., Niwa, Y., Noce, S., Pan, S., Parker, R. J., Peng, C., Ramonet, M., Riley, W. J., Rocher-Ros, G., Rosentreter, J. A., Sasakawa, M., Segers, A., Smith, S. J., Stanley, E. H., Thanwerdas, J., Tian, H., Tsuruta, A., Tubiello, F. N., Weber, T. S., van der Werf, G. R., Worthy, D. E. J., Xi, Y., Yoshida, Y., Zhang, W., Zheng, B., Zhu, Q., Zhu, Q., and Zhuang, Q.: Global Methane Budget 2000–2020, Earth Syst. Sci. Data, 17, 1873–1958, https://doi.org/10.5194/essd-17-1873-2025, 2025.

Simpson, D. and Darras, S.: Global soil NO emissions for Atmospheric Chemical Transport Modelling:

https://doi.org/10.5194/egusphere-2026-5718
Preprint. Discussion started: 15 October 2026
© Author(s) 2026. CC BY 4.0 License.

CAMS-GLOB-SOIL v2.2, Earth Syst. Sci. Data Discuss. https://doi.org/10.5194/essd-2021-221, 2021.

Sindelarova, K., Markova, J., Simpson, D., Huszar, P., Karlicky, J., Darras, S., and Granier, C.: High-resolution biogenic global emission inventory for the time period 2000–2019 for air quality modelling, Earth Syst. Sci. Data, 14, 251–270, https://doi.org/10.5194/essd-14-251-2022, 2022.

Soulie, A., Granier, C., Darras, S., Zilbermann, N., Doumbia, T., Guevara, M., Jalkanen, J.-P., Keita, S., Liousse, C., Crippa, M., Guizzardi, D., Hoesly, R., and Smith, S. J.: Global anthropogenic emissions (CAMS-GLOB-ANT) for the Copernicus Atmosphere Monitoring Service simulations of air quality forecasts and reanalyses, Earth Syst. Sci. Data, 16, 2261–2279, https://doi.org/10.5194/essd-16-2261-2024, 2024.

Stanevich, I., Jones, D. B. A., Strong, K., Parker, R. J., Boesch, H., Wunch, D., Notholt, J., Petri, C., Warneke, T., Sussmann, R., Schneider, M., Hase, F., Kivi, R., Deutscher, N. M., Velazco, V. A., Walker, K. A., and Deng, F.: Characterizing model errors in chemical transport modeling of methane: impact of model resolution in versions v9-02 of GEOS-Chem and v35j of its adjoint model, Geosci. Model Dev., 13, 3839–3862, https://doi.org/10.5194/gmd-13-3839-2020, 2020.

Stecher, L., Winterstein, F., Dameris, M., Jöckel, P., Ponater, M., and Kunze, M.: Slow feedbacks resulting from strongly enhanced atmospheric methane mixing ratios in a chemistry–climate model with mixed-layer ocean, Atmos. Chem. Phys., 21, 731–754, https://doi.org/10.5194/acp-21-731-2021, 2021.

Stevenson, D. S., Doherty, R. M., Sanderson, M. G., Collins, W. J., Johnson, C. E., and Derwent, R. G.: Radiative forcing from aircraft NOx emissions: Mechanisms and seasonal dependence, J. Geophys. Res., 109, D17307, https://doi.org/10.1029/2004JD004759, 2004.

Stevenson, D. S., Derwent, R. G., Wild, O., and Collins, W. J.: COVID-19 lockdown emission reductions have the potential to explain over half of the coincident increase in global atmospheric methane, Atmos. Chem. Phys., 22, 14243–14252, https://doi.org/10.5194/acp-22-14243-2022, 2022.

Stevenson, D. S., Zhao, A., Naik, V., O'Connor, F. M., Tilmes, S., Zeng, G., Murray, L. T., Collins, W. J., Griffiths, P. T., Shim, S., Horowitz, L. W., Sentman, L. T., and Emmons, L.: Trends in global tropospheric hydroxyl radical and methane lifetime since 1850 from AerChemMIP, Atmos. Chem. Phys., 20, 12905–12920, https://doi.org/10.5194/acp-20-12905-2020, 2020.

Szopa, S., Balkanski, Y., Schulz, M., Bekki, S., Cugnet, D., Fortems-Cheiney, A., Turquety, S., Cozic, A., D´eandreis, C., Hauglustaine, D., Idelkadi, A., Lathi`ere, J., Lef`evre, F., Marchand, M., Vuolo, R., Yan, N., and Dufresne, J.-L.: Aerosol and ozone changes as forcing for climate evolution between 1850 and 2100, Clim. Dynam., https://doi.org/10.1007/s00382-012-1408-y, 2013.

Turner, A. J., Jacob, D. J., Benmergui, J., Wofsy, S. C., Maasakkers, J. D., Butz, A., Hasekamp, O., and Biraud, S. C.: A large increase in U.S. methane emissions over the past decade inferred from satellite data and surface observations, Geophys. Res. Lett., 43, 2218–2224, https://doi.org/10.1002/2016GL067987, 2016.

van der Werf, G. R., Randerson, J. T., Giglio, L., van Leeuwen, T. T., Chen, Y., Rogers, B. M., Mu, M., van Marle, M. J. E., Morton, D. C., Collatz, G. J., Yokelson, R. J., and Kasibhatla, P. S.: Global fire emissions estimates during 1997–2016, Earth Syst. Sci. Data, 9, 697–720, https://doi.org/10.5194/essd-9-697-2017, 2017.

Voulgarakis, A., Naik, V., Lamarque, J.-F., Shindell, D. T., Young, P. J., Prather, M. J., Wild, O., Field, R. D., Bergmann, D., Cameron-Smith, P., Cionni, I., Collins, W. J., Dalsøren, S. B., Doherty, R. M., Eyring, V., Faluvegi, G., Folberth, G. A., Horowitz, L. W., Josse, B., MacKenzie, I. A., Nagashima, T., Plummer, D. A., Righi, M., Rumbold, S. T., Stevenson, D. S., Strode, S. A., Sudo, K., Szopa, S., and Zeng, G.: Analysis of present day and future OH and methane lifetime in the ACCMIP simulations, Atmos. Chem. Phys., 13, 2563–2587, https://doi.org/10.5194/acp-13-2563-2013, 2013.

Wang, X., Jacob, D. J., Downs, W., Zhai, S., Zhu, L., Shah, V., Holmes, C. D., Sherwen, T., Alexander, B., Evans, M. J., Eastham, S. D., Neuman, J. A., Veres, P. R., Koenig, T. K., Volkamer, R., Huey, L. G., Bannan, T. J., Percival, C. J., Lee, B. H., and Thornton, J. A.: Global tropospheric halogen (Cl, Br, I) chemistry and its impact on oxidants, Atmos. Chem. Phys., 21, 13973–13996, https://doi.org/10.5194/acp-21-13973-2021, 2021.

Weber, J., Shin, Y. M., Staunton Sykes, J., Archer-Nicholls, S., Abraham, N. L., and Archibald, A. T.: Minimal climate impacts from short-lived climate forcers following emission reductions related to the COVID-19

https://doi.org/10.5194/egusphere-2026-5718
Preprint. Discussion started: 15 October 2026
© Author(s) 2026. CC BY 4.0 License.



pandemic, Geophys. Res. Lett., 47, e2020GL090326, https://doi.org/10.1029/2020GL090326, 2020.

Wild, O.: Modelling the global tropospheric ozone budget: exploring the variability in current models, Atmos. Chem. Phys., 7, 2643–2660, https://doi.org/10.5194/acp-7-2643-2007, 2007.

Wild, O. and Prather, M. J.: Excitation of the primary tropospheric chemical mode in a global three-dimensional model, J. Geophys. Res., 105, 24 647–24 660, https://doi.org/10.1029/2000JD900399, 2000.

Wild, O., Prather, M. J., and Akimoto, H.: Indirect long-term global radiative cooling from NOx emissions, Geophys. Res. Lett., 28, 1719–1722, https://doi.org/10.1029/2000GL012573, 2001.

Wild, O., Voulgarakis, A., O'Connor, F., Lamarque, J.-F., Ryan, E. M., and Lee, L.: Global sensitivity analysis of chemistry–climate model budgets of tropospheric ozone and OH: exploring model diversity, Atmos. Chem. Phys., 20, 4047–4058, https://doi.org/10.5194/acp-20-4047-2020, 2020.

Wilson, C., Chipperfield, M. P., Gloor, M., Parker, R. J., Boesch, H., McNorton, J., Gatti, L. V., Miller, J. B., Basso, L. S., and Monks, S. A.: Large and increasing methane emissions from eastern Amazonia derived from satellite data, 2010–2018, Atmos. Chem. Phys., 21, 10643–10669, https://doi.org/10.5194/acp-21-10643-2021, 2021.

Zhao, Z., Peng, C., Yang, Q., Meng, F.-R., Song, X., Chen, S., Epule, T. E., Li, P., and Zhu, Q.: Model prediction of biome-specific global soil respiration from 1960 to 2012, Earth's Future, 5, 715–729, https://doi.org/10.1002/2016EF000480, 2017.

Zhang, Z., Poulter, B., Feldman, A. F., Ying, Q., Ciais, P., Peng S., Li, X.: Recent intensification of wetland methane feedback. Nat. Clim. Chang. 13, 430–433. https://doi.org/10.1038/s41558-023-01629-0, 2023.

Zhao, Y., Saunois, M., Bousquet, P., Lin, X., Berchet, A., Hegglin, M. I., Canadell, J. G., Jackson, R. B., Deushi, M., Jöckel, P., Kinnison, D., Kirner, O., Strode, S., Tilmes, S., Dlugokencky, E. J., and Zheng, B.: On the role of trend and variability in the hydroxyl radical (OH) in the global methane budget, Atmos. Chem. Phys., 20, 13011–13022, https://doi.org/10.5194/acp-20-13011-2020, 2020.

Zhao, Y., Zheng, B., Saunois, M., Ciais, P., Hegglin, M. I., Lu, S., Li, Y., and Bousquet, P.: Air pollution modulates trends and variability of the global methane budget, Nature, 10.1038/s41586-025-09004-z, 2025.